

1 **Advance prediction of coastal groundwater levels with temporal**  
2 **convolutional and long short-term memory networks**

3 Xiaoying Zhang<sup>a,b</sup>, Fan Dong<sup>a,b</sup>, Guangquan Chen<sup>c</sup>, Zhenxue Dai<sup>a,b\*</sup>

4 <sup>a</sup> Institute of Intelligent Simulation and Early Warning for Subsurface Environment,  
5 Jilin University, Changchun, China

6 <sup>b</sup> College of Construction Engineering, Jilin University, Changchun, China

7 <sup>c</sup> Key Laboratory of Marine Sedimentology and Environmental Geology, First  
8 Institute of Oceanography, State Oceanic Administration, Qingdao, China

9 \* Correspondence: Zhenxue Dai, [dzx@jlu.edu.cn](mailto:dzx@jlu.edu.cn)

10

11 **Highlights**

- 12 • TCN- and LSTM-based models were proposed to predict groundwater levels in a  
13 coastal aquifer
- 14 • Tidal, precipitation and groundwater levels were utilized as input data in the  
15 networks
- 16 • In advance 1- day, 3-, 7- and 15-days groundwater levels were predicted with the  
17 highest accuracy of 1-day-lead prediction
- 18 • The TCN-based model slightly outperformed the LSTM-based model in accuracy  
19 but less efficiency

20

21 **Abstract**

22 Prediction of groundwater level is of immense importance and challenges for the  
23 coastal aquifer management with rapidly increasing climatic change. With the  
24 development of artificial intelligence, the data driven models have been widely adopted  
25 in hydrological processes management. However, due to the limitation of network  
26 framework and construction, they are mostly adopted to produce only one-time step in  
27 advance. Here, the temporal convolutional network (TCN) and long short-term memory

28 (LSTM) based models were developed to predict groundwater levels with different  
29 leading periods in a coastal aquifer. The beginning hourly-monitored ten-month data in  
30 two monitoring wells were used for model training and testing, and the data of the  
31 following three months were used as prediction with 24, 72, 180 and 360 time steps (1-  
32 day, 3-, 7- and 15-days) in advance. The historical precipitation and tidal level data  
33 were incorporated as input data. For one-step prediction of the two wells, the calculated  
34  $R^2$  of the TCN-based models values were higher and the RMSE values were lower than  
35 that of the LSTM-based model in the prediction stage with shorter running times. For  
36 the advanced prediction, the model accuracy decreased with the increase of advancing  
37 period from 1-day to 3-, 7- and 15-days. By comparing the simulation accuracy and  
38 efficiency, the TCN-based model slightly outperformed the LSTM-based model but less  
39 efficient in training time. Both models showed great ability to learn complex patterns  
40 in advance using historical data with different leading periods, and had been proved to  
41 be valid localized groundwater level prediction tools in the subsurface environment.

42

43 **Keywords:** prediction; Groundwater level; Coastal aquifer; Temporal convolutional  
44 networks; Long Short-Term Memory

45

46

47

## 48 **1 Introduction**

49 As the economic development and population escalate in coastal area, the fresh

50 groundwater needs continue to mount, seawater intrusion has post great threat to the  
51 availability of portable water resources globally (Baena-Ruiz et al., 2018). In United  
52 States, Mexico, Canada, Australia, China, India, South Korea, Italy and Greece with  
53 dense population, many coastal aquifers have experienced salinization caused by  
54 seawater intrusion (Barlow and Reichard, 2009; Park et al., 2011; Pratheepa et al., 2015;  
55 Zhang et al., 2017; Lu et al., 2013). Protection projects such as aquifer replenishment  
56 can be constructed to alleviate seawater intrusion by artificially increasing groundwater  
57 recharge in the aquifer than what occurs naturally (Abdalla and Al-Rawahi, 2012; Lu  
58 et al., 2019). The replenishment programs have been operated in developed area such  
59 as Perth, Western Australia, and California, USA (Garza-Díaz et al., 2019). The  
60 infrastructures tend to be costly and out of reach for many developing countries. A  
61 reliable seawater intrusion monitoring and predicting system is still essential and is  
62 recognized as the most effective way of keeping freshwater water from contamination  
63 of seawater (Xu and Hu, 2017).

64 In the past several decades, conventional numerical models have been widely  
65 utilized to simulate and predict the groundwater fluctuation dynamics and chemical  
66 variations (Batelaan et al., 2003; Dai et al., 2020; Huang et al., 2015; Li et al., 2002).  
67 However, the difficulty of acquiring extensive hydrological and geological data and  
68 setting reasonable boundaries limits its application on seawater intrusion management.  
69 Meanwhile, the method is not suitable to simultaneously adopt updated monitoring data  
70 and produce real-time prediction. Under such circumstances, where data source is  
71 scarce, artificial intelligence technology has been proposed in groundwater dynamic

72 prediction. Artificial neural network (ANN) has been greatly improved and became a  
73 robust tool for dealing groundwater problems, where the flow is nonlinear and highly  
74 dynamic in nature (Maier and Dandy, 2000). The conventional network model generally  
75 has defects such as high computational complexity, slow training speed, and failure in  
76 retaining historical information, thus is hardly to be enrolled in the long-term time-  
77 series prediction (Cannas et al., 2006; Mei et al., 2017). To solve this problem,  
78 researchers upgraded the conventional networks by integrating them with methods like  
79 genetic algorithm (Danandeh Mehr and Nourani, 2017; Ketabchi and Ataie-Ashtiani,  
80 2015), singular spectrum (Sahoo et al., 2017), and wavelet transform (Gorgij et al., 2017;  
81 Seo et al., 2015; Zhang et al., 2019). Singular spectrum analysis and wavelet transform  
82 can help to preprocess the time-series data before they are put into the neural networks  
83 to improve prediction accuracy and efficiency.

84 With the computing capacity development, deep learning (DL) has emerged as a  
85 very powerful time-series prediction method. DL models are particularly suitable for  
86 big data time-series, because they can automatically extract complex patterns without  
87 feature extraction preprocessing steps (Torres et al., 2019). However, the general fully  
88 connected networks are not effective to capture the temporal dependence of time-series  
89 (Senthil Kumar et al., 2005). Therefore, more specialized DL models, such as recurrent  
90 neural networks (RNN) (Rumelhart et al., 1986) and convolutional neural networks  
91 (CNN) (Lecun et al., 1998) have been adopted in the field of time-series prediction  
92 (Feng et al., 2020). Different from the back-propagation (BP) neural network that the  
93 information flows from the input to the output layer in one direction, the RNN preserves

94 the information from the previous step as input to the current step with loops (Coulibaly  
95 et al., 2001). This allows the RNN to handle time-series and other sequential data but  
96 generally is not straightforward for a long-term calculation in practice (Bengio et al.,  
97 1994). Therefore, the enhanced RNN model, long short-term memory (LSTM) is  
98 proposed and capable to process high variable-length sequences even with millions of  
99 data points (Fischer and Krauss, 2018; Kratzert et al., 2019) . As one of the best deep  
100 neural network model in time-series predicting, the LSTM has been widely used in the  
101 prediction of temporal variations such as stock market predictions (Fischer and Krauss,  
102 2018), rainfall-runoff (Kumar Dubey et al., 2021) and groundwater level (Solgi et al.,  
103 2021). Despite of substantial progresses in hydrology predicting, these networks still  
104 have issues of low training efficiency and low accuracy (Zhan et al., 2022).

105 More recently, a variant of the CNN architecture known as temporal convolutional  
106 networks (TCN) has acquired popularity (Bai et al., 2018). The prominent characteristic  
107 of TCN is its ability to capture long-term dependencies without information loss (Cao  
108 et al., 2021). Meanwhile, it joints a residual block structure to fix the disappearance of  
109 gradient in the deep network structure (Chen et al., 2020). With proper modifications,  
110 the TCN is quite genetic and easily to be used to build a very deep and extensive  
111 network in sequence modeling. In earth science, the TCN has been successfully applied  
112 to time-series prediction tasks including multivariate time-series predicting for  
113 meteorological data (Wan et al., 2019), probabilistic predicting (Chen et al., 2020) and  
114 wind speed predicting (Gan et al., 2021). Researches suggest that the TCN convincingly  
115 has advantage in popular deep learning models across a broad range of sequence

116 modeling tasks (Borovykh et al., 2019; Chen et al., 2020; Wan et al., 2019). Another  
117 import subject is that these networks are mostly used to predict variables in only one  
118 step, which is not enough for the prediction of hydrology information in management.  
119 Researches have been adopted the method to predict the trends of ENSO and sea  
120 temperature (Yan et al.,2020; Jian et al., 2021). However, the potential of TCN has not  
121 been investigated in the sequencing model of hydrogeology field. Therefore, it is  
122 worthy to explore their prediction abilities in leading periods.

123 The objective of this study is to develop real-time advance prediction climate-  
124 dydro hybrid data-driven models of groundwater level in the coastal aquifer based on  
125 TCN and LSTM. The hourly processed tidal, precipitation with groundwater level data  
126 in monitoring wells of Laizhou Bay are utilized to train model and predict the  
127 groundwater level in a period of 1-day, 3-,7- and 15-days. The two models were further  
128 compared in the view of accuracy and efficiency. The rest of the paper is organized as  
129 follows. Sect. 2 introduces the study area and observational data. Sect. 3 illustrates the  
130 detailed concepts of TCN and LSTM, the experimental model settings and model  
131 evaluation criteria. Sect. 4 presents the predicting results and discussions. Finally, the  
132 paper is concluded in Sect. 5.

## 133 **2 Study area and data processing**

### 134 **2.1 Site description**

135 The study area is located in the south coast of Laizhou Bay, along the Yangzi to  
136 Weifang section in Shandong province of China (Fig. 1). The Laizhou Bay is one of the  
137 earliest and most seriously affected area by seawater intrusion since 1970s in China

138 (Han et al., 2014; Zeng et al., 2016). The area is a coastal plain, which contains a series  
139 of Cretaceous to modern sediments that covering the Paleozoic basement. The  
140 sedimentary facies of coastal aquifer are alluvium, proluvial and marine sediments from  
141 south to north (Han et al., 2011). According to the research of (Xue et al., 2000), there  
142 were three seawater intrusion and regression events in the sea area of Laizhou Bay since  
143 the upper Pleistocene. The transgression in the early upper Pleistocene formed the third  
144 marine aquifer containing sedimentary water. These brine were formed by evaporation  
145 and concentration of ancient seawater and re-dissolution and mixing of salt (Dai and  
146 Samper, 2006; Zhang et al., 2017). The monitoring wells BH01-BH05 are distributed  
147 in the study area along a cross section perpendicular to the coastline. Among the wells,  
148 the well BH01 and BH05 have relatively integrate data in time and distributed in the  
149 two sides of the cross profile with distinguished annual variation pattern, which are  
150 selected as examples for the developed models.



151

152 Figure 1. Schematic figure of the study area with monitoring wells BH01-BH05.

## 153 **2.2 Data collection and pre-processing**

154 The precipitation and tidal level are selected as the primary factors to affect the  
155 groundwater dynamics in the coastal area. The data in the period of 2011 to 2012 with  
156 groundwater level observations of two wells are combined as the input of the deep  
157 learning models. A total of 28,836 data items are collected for monitoring wells and the  
158 variations of groundwater level, and tidal level with precipitation are shown in Figure  
159 2. The rainfall is concentrated from June to September and in shortage from December  
160 to April. The tide in the study area is irregular mixed with a semi-diurnal variation. In  
161 the experiments, ten months of data from October 2011 to July 2012 is first extracted  
162 for model training and testing. The rest of the data from August 2012 to October 2012  
163 is used to test model prediction accuracy.

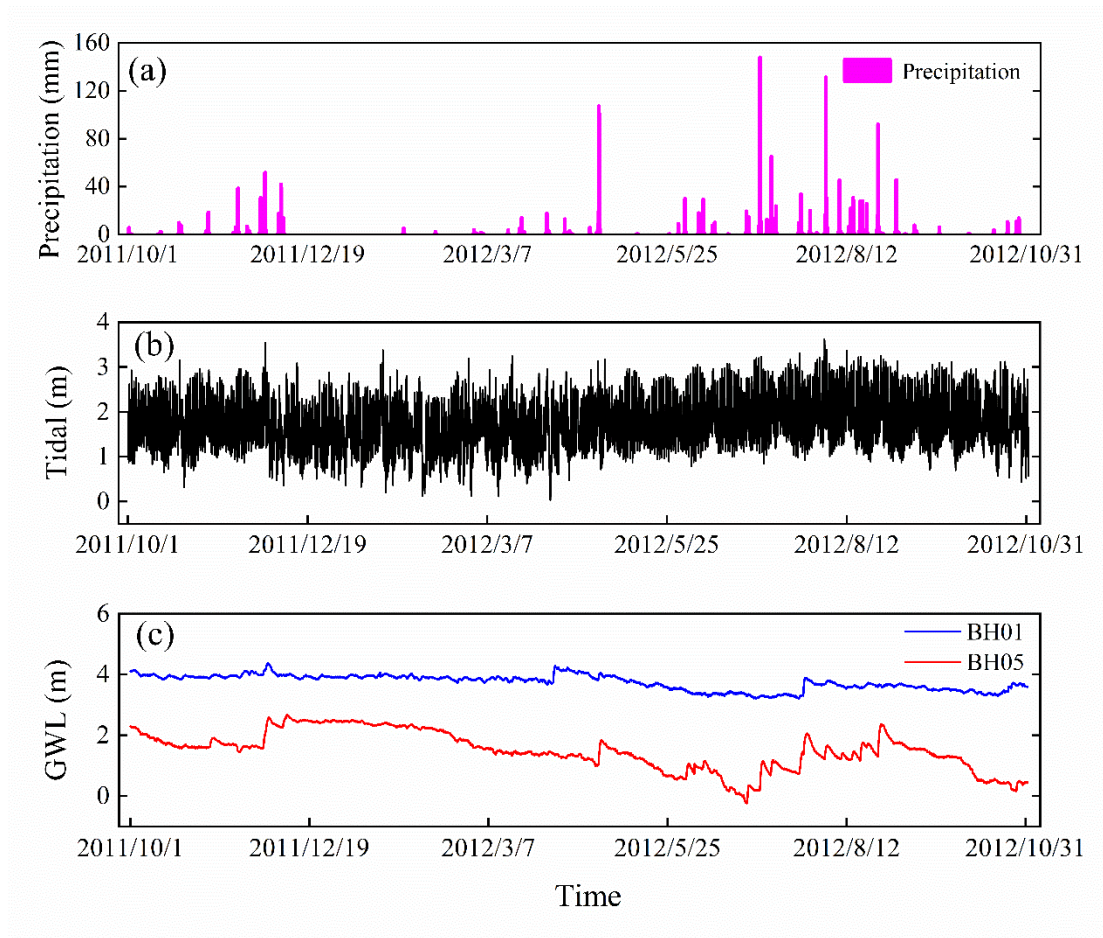
164 In addition, the magnitudes of meteorological and hydrological variables have  
165 obvious temporal variations. To reduce the negative impact on the model learning  
166 ability, especially on the speed of gradient descent, all variables are normalized to  
167 ensure that they remain at the same scale (Kratzert et al., 2019). This pre-processing  
168 method ensures the stable convergence of parameters in the developed TCN- and  
169 LSTM-based models and improve the simulation accuracy of the model. The  
170 normalization formula is as follows:

$$171 \quad x'_{i_i} = \frac{x_i - x_{min}}{x_{max} - x_{min}} \quad (1)$$

172 where  $x_i$  represents the original data in time  $i$  and  $x_i$  represents the original data in time  
173  $i$   $x_{max}$  and  $x_{min}$  are the maximum and minimum variable values. The output of the



174 network is retransformed to obtain the final groundwater level prediction, which is an  
175 inverse data scaling process.



176  
177 Figure 2. Time-series of the variables in the study, including (a) precipitation, (b) tide,  
178 (c) groundwater level (GWL).

### 179 **3 Methodology**

#### 180 **3.1 Temporal Convolutional Network**

181 The TCN is first proposed for video action segmentation and detection by  
182 hierarchically capturing intermediate feature presentations. Then the term is extended  
183 for sequential data for a wide family of architectures with generic convolution (Bai et  
184 al., 2018; Lea et al., 2017). Suppose that we have an input hydro-climate sequence at  
185 different times  $x_0, \dots, x_T$ , the goal of the modeling is to predict the corresponding

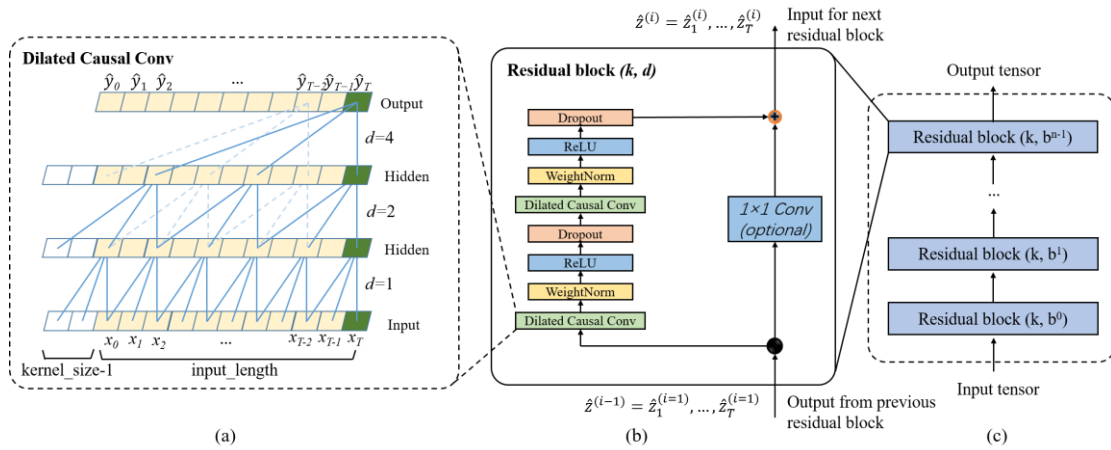
186 groundwater level as outputs  $y_0, \dots, y_T$  at each time. The problem could transfer to build  
187 a network  $f$  that minimizes the function loss between observations and actual network  
188 outputs  $L[(y_0, \dots, y_T), (\hat{y}_0, \dots, \hat{y}_T)]$ , where  $\hat{y}_0, \dots, \hat{y}_T = f(x_0, \dots, x_T)$ . Currently, a typical  
189 TCN consists of dilated, causal 1D full-convolutional layers with the same input and  
190 output lengths. With TCN, the prediction  $y_t$  depends only on the data from  $x_0$  and  $x_t$  and  
191 not include the future data from  $x_t$  and  $x_T$  (Yan et al., 2020). With the three key  
192 components of TCN, it has two distinguishing characteristics: (1) the TCN is able to  
193 map the same length of output as the input sequence as in RNN; (2) the convolution  
194 involved in TCN is causal, eliminating the influence of future information on the output.

### 195 3.1.1 Causal Dilated Convolutions

196 In the TCN, the first advantage is accomplished by a 1D full-convolutional network  
197 (FCN) architecture. Different from the traditional CNN, the FCN transforms the fully  
198 connected layers into the convolutional layers for the last layers, preserving the same  
199 length of output as that of the input (Long et al., 2015). As shown in Fig. 3a, the lengths  
200 of the input, the hidden and the output layers are the same in the FCN. Some zero  
201 padding is needed in this step by adding additional zero-valued entries with a length of  
202 kernel size-1 in each layer. The kernel size is the number of successive elements that  
203 are used to produce one element in the next layer.

204 To avoid the information leakage from the future (after time  $t$ ), the TCN uses  
205 causal convolution instead of standard convolution, where only the elements at or  
206 before time  $t$  in the previous layer are adopted into the mapping of the output at time  $t$ .  
207 Further, the dilated convolution is employed to capture long-term historical information

208 by skipping a given step size (dilation factor  $d$ ) in each layer. For example, the dilation  
 209 factor  $d$  increases from 1 to 4 with the evolution of the network depth ( $n$ ) in an  
 210 exponential increasing pattern. In this way, a very large receiving domain is created and  
 211 all the historical records in the input can be involved in the prediction model with a  
 212 deep network.



213  
 214 Figure 3. Architectural elements in the proposed TCN. (a) the structure of causal dilated  
 215 convolution; (b) the TCN residual block. An  $1 \times 1$  convolution is added when residual  
 216 input and output have different dimensions; (c) framework of residual connection in the  
 217 TCN.

### 218 3.2.2 Residual Connections

219 In a high dimensional and long-term sequence, the network structure could be very  
 220 deep with increasing complicity and cause a vanishing gradient. To solve this issue, a  
 221 residual block structure is introduced to replace the simple 1D causal convolution layer,  
 222 so that the designed TCN structure is more generic (He et al., 2016). The residual block  
 223 in a TCN is represented in Fig. 3b. It has two convolutional layers with the same kernel  
 224 size and dilation factor and non-linearity. To solve non-linear models, the rectified

225 linear unit (ReLU) is added to the top of the convolutional layer (Nair and Hinton, 2010).  
226 The weight normalization is applied between the input of hidden layers (Salimans and  
227 Kingma, 2016). Meanwhile, a dropout is added after each dilated convolution for  
228 regularization (Srivastava et al., 2014). For all connected inner residual blocks, the  
229 channel widths of input and output are consistent. But the width may be different  
230 between the input of the first convolutional layer of the first residual block and the  
231 output of the second convolutional layer of the last residual block. Therefore, a  $1 \times 1$   
232 convolution is added in the first and last residual block to adjust the dimensions of the  
233 residual tensor into the same. The output of the residual block is represented by  $\hat{Z}^{(i)}$  for  
234 the  $i^{\text{th}}$  block.

### 235 3.2.3 Structure of TCN

236 A complete structure of TCN is illustrated in Fig.3c. It contains a series of  
237 proceeding residual blocks. The structural characteristics make TCN a deep learning  
238 network model very suitable for complex time-series prediction problems (Lara-  
239 Benítez et al., 2020). The main advantage of TCN is that, similar to RNN, they have  
240 flexible receptive fields and can deal with various length input by sliding one-  
241 dimensional causal convolution kernel. Furthermore, because TCN shares a  
242 convolution kernel and has parallelism, it can process long sequences in parallel instead  
243 of sequential processing like RNN, so it has lower memory usage and shorter  
244 computing time than a cyclic network. Moreover, RNN often has the problems of  
245 gradient disappearance and gradient explosion, which are mainly caused by sharing  
246 parameters in different periods, while TCN uses a standard backpropagation-through-

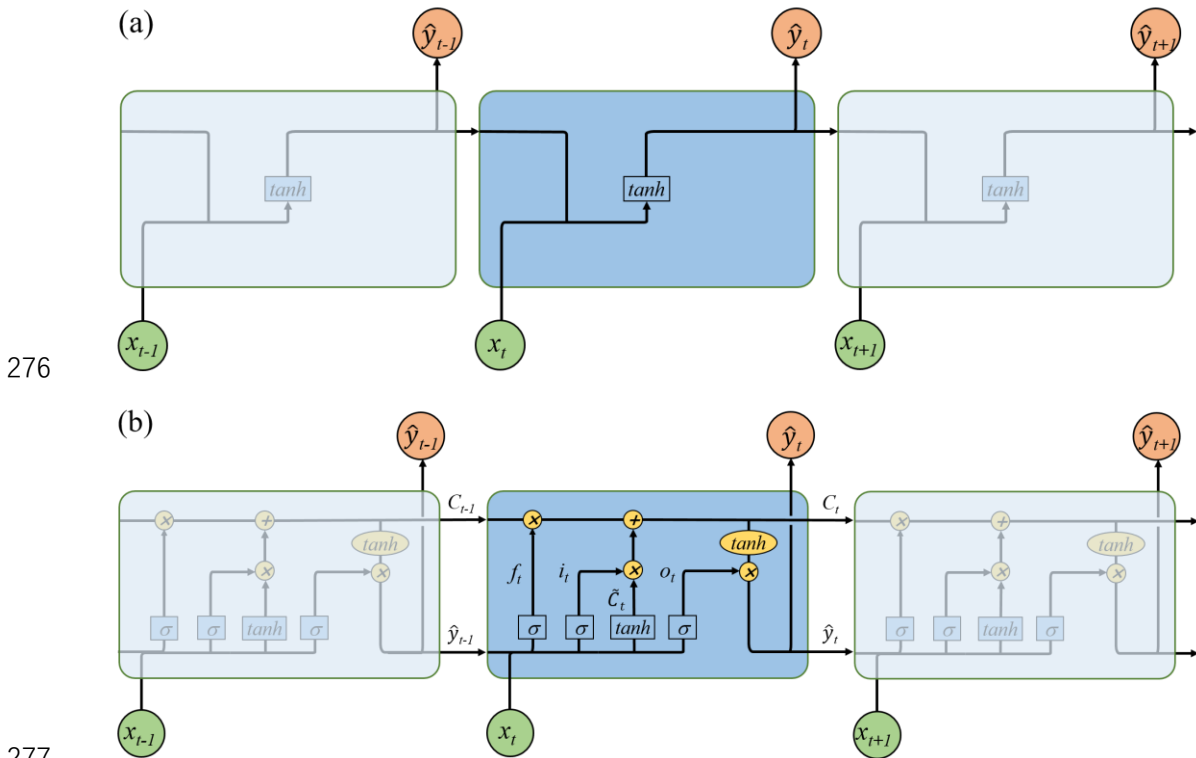
247 time algorithm (BPTT) for training, so there is little gradient disappearance and  
248 explosion problem (Pascanu et al., 2012). The detailed mathematical calculation and  
249 associated information of the TCN architecture are referred to (Bai et al., 2018).

### 250 **3.2 Long Short-Term Memory network**

251 LSTM is a special RNN model explicitly designed for long-term dependence  
252 problems. As shown in Fig. 4a, the RNN has a series of repeating modules that  
253 recursively connected in the evolution direction of the sequence. The chain-like  
254 structure permits the RNN to retain important information in a “tanh” layer and produce  
255 the same length of output  $\hat{y}_t$  as input  $x_t$ . However, the short-length “remember time” is  
256 not enough for the groundwater prediction. Especially for our hourly recorded data, a  
257 maximum step about ten reported by Bengio et al. (1994) is unable to count the effect  
258 of annually, seasonally, and even daily groundwater variation. Different from the simple  
259 layer in the RNN, the LSTM has a more complicated repeating module with four  
260 interacting layers.

261 The core idea of LSTM is the special structure to control the cell state in the  
262 module as shown in Fig. 4b. It includes a cell and an input gate  $i_t$ , a forget gate  $f_t$ , and  
263 an output gate  $o_t$ . The information can directly flow down along cells  $C$  without critical  
264 changes, therefore, preserving long-term history messages (Zhang et al., 2018b). The  
265 three gates control which data in a sequence is important to keep or throw away, and  
266 protect the relevant information passed down in the cell to make predictions. The forget  
267 gate  $f_t$  has a sigmoid layer to determine which information is discarded with a value  
268 between 0 and 1. The lower the value, the less the information added to the cell state

269 (Ergen and Kozat, 2018). Opposite the forget gate, the input gate  $i_t$  decides what  
 270 information to retain in the cell state. It is composed of two parts: a sigmoid layer and  
 271 a tanh layer. The two layers are combined to govern which values will be updated by  
 272 generating a new candidate value  $\tilde{C}_t$ . The old cell state  $C_{t-1}$  then can be updated into  
 273 the new cell state  $C_t$  with a weighted function. Finally, the output gate  $o_t$  determines  
 274 what parts of the cell state should be passed on to the next hidden state. The detailed  
 275 calculation of the LSTM can be referenced to (Lea et al., 2016).



278 Figure 4. Graphical representation for (a) chain like structure of the RNN by assigning  
 279  $x_t$  and  $\hat{y}_t$  as input and output. The self-connected hidden units allow information to be  
 280 passed from one step to the next; (b) LSTM's memory block based on RNN. The  
 281 hidden block includes three gates (input  $i_t$ , forget  $f_t$ , output  $o_t$ ) and a cell state to select  
 282 and pass the historical information.

### 283 **3.3 Experimental study**

284 The TCN- and LSTM-based models were developed separately for monitoring  
285 wells BH01 and BH05. Due to the high complexity of the DL models, setting  
286 appropriate hyper-parameters for the developed networks is very important. Here, the  
287 impact of the size of the input window, the epoch number and the batch size were tested  
288 with different convolutional architectures over the monitoring data (Lara-Benítez et al.,  
289 2020). The learning dataset is first divided into two parts: 80% of the time-series data  
290 is used as training set, and 20% of the data is utilized as testing set. The effect of  
291 different splitting strategies is further tested in section 4. With the increase of the epoch  
292 numbers, the curve gradually approaches to the optimal fitting state from the initial non-  
293 fitting state, but too many epochs frequently lead to over-fitting of the neural network  
294 (Afaq and Rao, 2020). Meanwhile, the number of iterations generally increases for  
295 updating weights in the neural network. Therefore, the number of epoch from 0 to 300  
296 is evaluated. Batch size represents the number of samples between model weight  
297 updates (Kreyenberg et al., 2019). The value of the batch size often is set between 1  
298 and hundreds. Larger batch size often leads to faster convergence of the model, but may  
299 lead to less ideal of the final weight set. To find the best balance between memory  
300 efficiency and capacity, the batch size should be carefully set to optimize the  
301 performance of the network model. Besides these parameters, the number of filters in  
302 the TCN-based and the hidden nodes in the LSTM-based model were as well tested  
303 within reasonable ranges.

304 The 1-day, 3-, 7-, and 15-days leading prediction experiments were further

305 conducted to test the capacity of DL methods in predicting long-term groundwater level  
 306 in the coastal aquifer. To eliminate the randomness of model training, all experiments  
 307 were repeated 5 times and the average values of each index were compared. In all  
 308 experiments, the average absolute error (MAE) has been used as the loss function of  
 309 networks (Lara-Benítez et al., 2020). The Adam optimizer has an adaptive learning rate,  
 310 which can improve the convergence speed of deep networks, which has been used to  
 311 train the models (Kingma and Ba, 2015).

### 312 **3.4 Evaluation of model performance**

313 Two evaluation metrics, coefficient of determination ( $R^2$ ) and root mean square  
 314 error (RMSE) are selected to quantify the goodness-of-fit between model outputs and  
 315 observations (Zhang et al., 2020). The two criteria are calculated using the following  
 316 equations:

$$317 \quad RMSE = \sqrt{\frac{1}{N} \sum_{i=1}^N (h_i - y_i)^2} \quad (1)$$

$$318 \quad R^2 = \frac{\sum_{i=1}^N (h_i - \bar{h})^2 - \sum_{i=1}^N (h_i - y_i)^2}{\sum_{i=1}^N (h_i - \bar{h})^2} \quad (2)$$

319 where  $h_i$  is the observed groundwater level at time  $i$ ,  $y_i$  is the network prediction values  
 320 at time  $i$ ,  $\bar{h}$  is mean of the observed groundwater levels, and  $n$  is the number of  
 321 observations. RMSE measures the prediction precision which creates a positive value  
 322 by squaring the errors. The RMSE score is between  $[0, \infty]$ . If the RMSE approaches to  
 323 0, the model prediction is ideal.  $R^2$  measures the degree of model replication results,  
 324 ranging between  $[-\infty, 1]$ . For the optimal model prediction, the score of  $R^2$  is close to  
 325 1.



## 326 **4 Results and discussions**

### 327 **4.1 Hyper-parameter trial experiments**

#### 328 4.2.1 Experiments of the TCN-based model

329 The TCN-based model was built on Keras platform using TensorFlow of python  
330 as the backend. Taken the groundwater level prediction data set in well BH01 as an  
331 example, the trials were set up with a variety combination of different hyper-parameters  
332 in the TCN-based model as illustrated in Table 1. With the fixed number of epoch, the  
333 simulation results of 32 filters were better than that of 16 and 64 filters. Meanwhile,  
334 under the condition of 32 filters, the accuracy of the model decreased with the  
335 increasing of batch size. The results of the 16 batch size were better than that of 32  
336 and 64 batches. Based on the above experimental results, the influence of different  
337 numbers of epoch on the simulation was further explored with the filters was 32 and  
338 the batch size was 16 as shown in Fig.5. The overall results of the model were improved  
339 when the number of epoch increased from 100 to 190 though the variation was not  
340 strictly linear, and the variations became stable with minor fluctuations when the  
341 number of epoch exceeded 200.

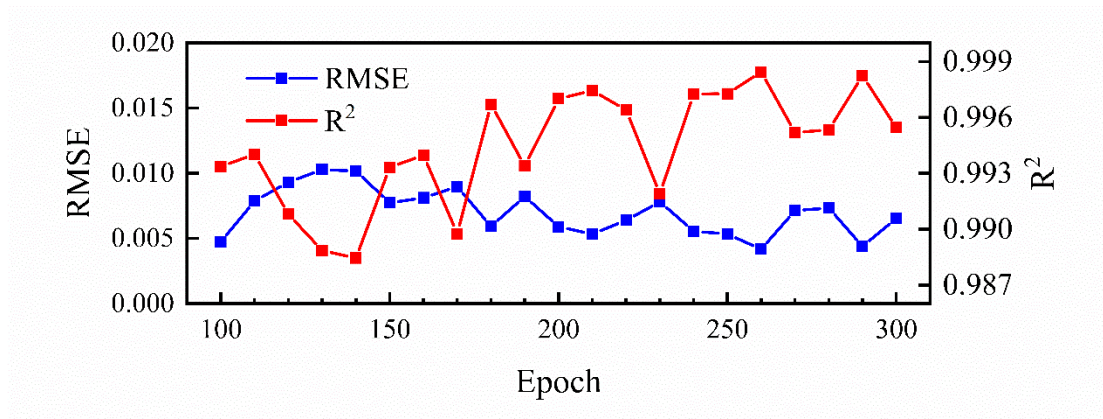
342 Table 1. The RMSE and  $R^2$  values between the observed and predicted groundwater  
343 levels in well BH01 with different numbers of epochs, different numbers of filters, and  
344 different batch sizes. The bold values represent the optimal hyper-parameters with the  
345 smallest RMSE and the highest  $R^2$  scores in the TCN-based model.

346

Epoch	Filters	Batch size	RMSE(m)	$R^2$	Time(min)
		16	0.0182	0.9904	1.29

100	32	32	0.0117	0.9876	1.05
		64	0.0117	0.9875	0.78
200	16	16	0.0078	0.9946	2.41
		32	0.0068	0.9959	1.75
		64	0.0090	0.9942	1.19
<b>200</b>	<b>32</b>	<b>16</b>	<b>0.0059</b>	<b>0.9970</b>	2.58
		32	0.0075	0.9948	2.01
		64	0.0082	0.9938	1.51
200	64	16	0.0125	0.9906	3.68
		32	0.0101	0.9907	3.21
		64	0.0157	0.9775	2.76
300	32	16	0.0065	0.9955	3.8
		32	0.0076	0.9946	3.01
		64	0.0099	0.9904	2.22

347



348

349 Figure 5. The variation of RMSE and  $R^2$  values between the observed and predicted  
350 groundwater levels of well BH01 with the increasing number of epoch when the number  
351 of filters is 32 and the batch size is 16.

#### 352 4.2.2 Experiments of the LSTM-based model

353 The number of epochs and hidden nodes are two key parameters affecting the  
354 simulation accuracy of LSTMs (Zhang et al., 2018a). Different hyper-parameter

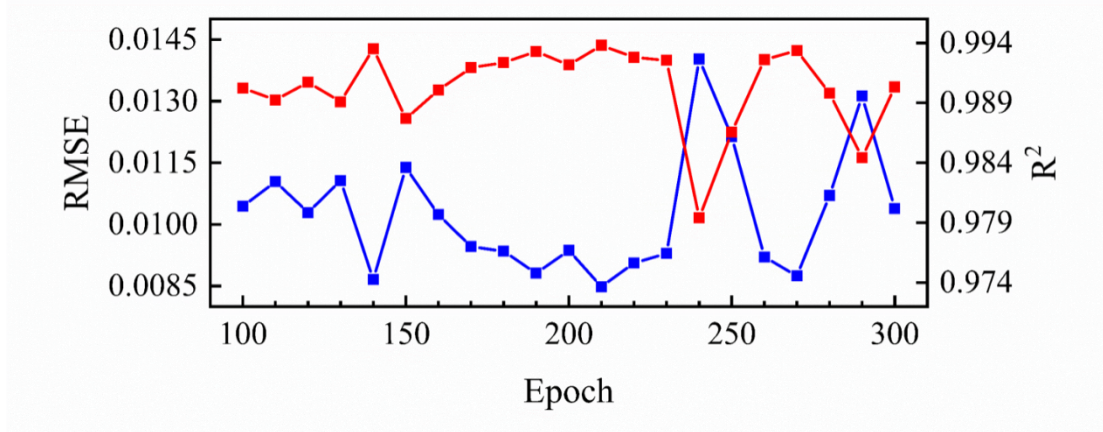
355 combinations were tested as well as in the proposed TCN-based model with  
 356 groundwater levels in well BH01. The RMSE,  $R^2$  and running time are shown in Table  
 357 2. With a fixed number of hidden nodes, the results of 100 and 200 epochs were better  
 358 than that in the 300 epochs experiment. A detailed variation of RMSE and  $R^2$  values  
 359 with increasing number of hidden nodes and epochs is further illustrated in Fig. 6. The  
 360 figure shows that the RMSE and  $R^2$  have a decreasing and increasing trend separately  
 361 when the number of epochs is greater than 150, but is reversed when it is larger than  
 362 240. The variations of RMSE and  $R^2$  with increasing hidden nodes have similar changes  
 363 as shown in Table 2. Though an insufficient number of neurons may decrease the  
 364 learning ability of the network, the results indicate that an increasing training hyper-  
 365 parameters may not necessary to ensure better prediction.

366 Table 2. The RMSE and  $R^2$  values between the observed and predicted groundwater  
 367 levels in well BH01 with different numbers of epochs and hidden nodes. The bold  
 368 values represent the optimal hyper-parameters used in the proposed LSTM-based  
 369 model.

Epoch	Hidden nodes	RMSE	$R^2$	Time(min)
100	50	0.0104	0.9902	1.01
	60	0.0098	0.9916	1.38
	70	0.0095	0.9922	1.53
	80	0.01	0.9913	1.75
<b>200</b>	50	0.0094	0.9922	1.91
	60	0.0089	0.9931	2.59
	<b>70</b>	<b>0.0088</b>	<b>0.9932</b>	<b>2.96</b>
	80	0.0092	0.9925	3.28
300	50	0.0101	0.9903	2.86
	60	0.0105	0.9901	3.85

70	0.0103	0.9907	4.29
80	0.0120	0.9872	4.92

370



371

372 Figure 6. The variation of RMSE and R<sup>2</sup> values between the observed and predicted  
373 groundwater levels of well BH01 with the increasing of the number of epochs when the  
374 hidden node is 50.

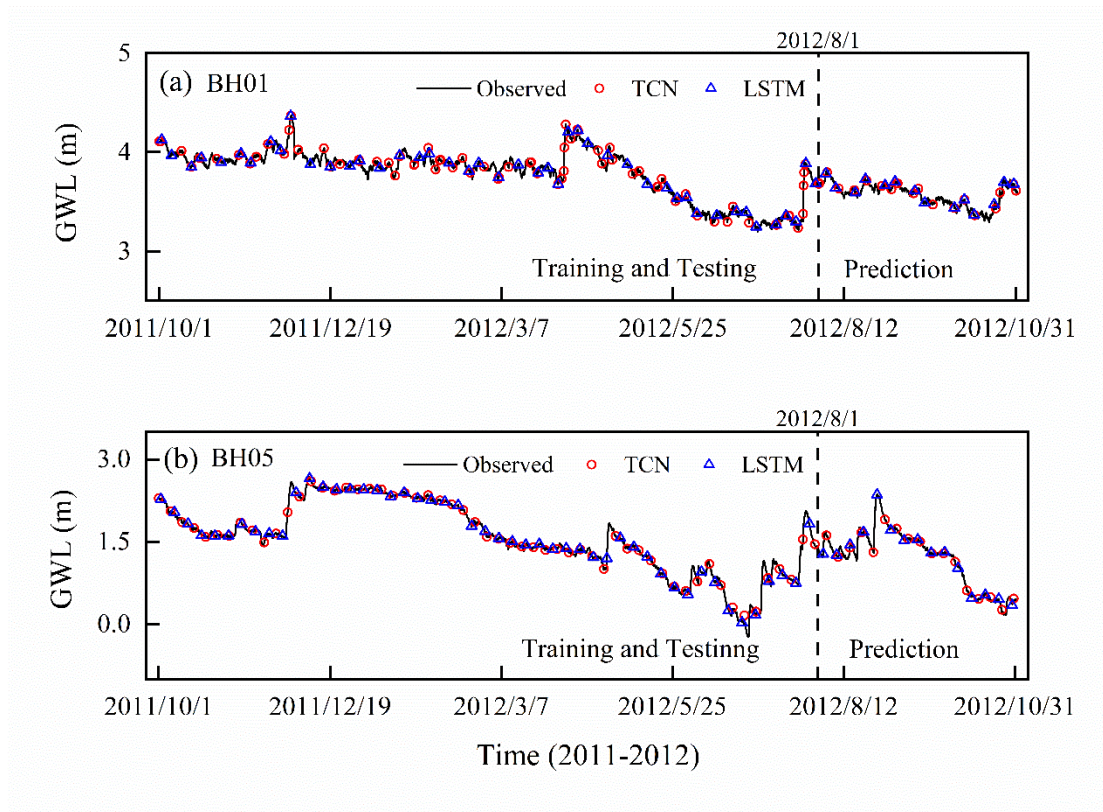
375 The trial experimental results present similar fitting pattern shared by the two kind  
376 of networks. The growing value of parameters dramatically increases the computational  
377 cost in the network. For example, the time cost from 50 to 80 hidden nodes has  
378 increased about 1.7 times in each iteration trial in the LSTM-based model. Finally, 200  
379 epochs, 32 filters, and the 16 batch size were chosen as the optimal parameters in the  
380 TCN network. For the LSTM network, the number of epoch and hidden nodes were  
381 chosen as 200 and 70.

### 382 4.3 Model performance and evaluation

383 The optimal hyper-parameters of the proposed TCN-based model for  
384 groundwater level predicting are shown in Table 1 (epoch = 200, filters = 32 and batch  
385 size = 16). Besides that, the kernel size in each convolutional layer is set as 6, the

386 dilations are [1,2,4,8]. For the LSTM-based model, the batch size is set to 148 with  
387 epoch=200 and nodes=70. The same hyper-parameters are then utilized to construct  
388 TCN and LSTM architectures for prediction of groundwater level in different  
389 monitoring wells.

390 The one step ahead simulated groundwater level in the training and testing, and  
391 prediction stages by the two models are shown in Fig. 7. For both models, the simulated  
392 values completely capture the variation of groundwater levels in monitoring wells with  
393 overlapped plot. The  $R^2$  and RMSE values of simulation results are listed in Table 3. In  
394 the prediction stage, the values of RMSE are 0.0019 and 0.0166 for BH01 and BH05,  
395 and the values of  $R^2$  are larger than 0.999 in the prediction for the TCN-based model.  
396 For the LSTM-based model, the RMSE values are 0.0074 and 0.0588, and the  $R^2$  values  
397 are 0.9957 and 0.9980. These metrics indicate that both models can “remember” the  
398 historical records and produce true observations. The simulation accuracy of TCN-  
399 based models is slightly higher than the LSTM-based models. In addition, the running  
400 time of the TCN-based model is 2.6 minutes, which is faster than that of the TCN-based  
401 model.



402

403 Figure 7. The simulation results of groundwater level of monitoring wells BH01 and  
 404 BH05 by TCN-based model. The black dash line divides the data into two groups: the  
 405 training and testing dataset, and the prediction dataset.

406

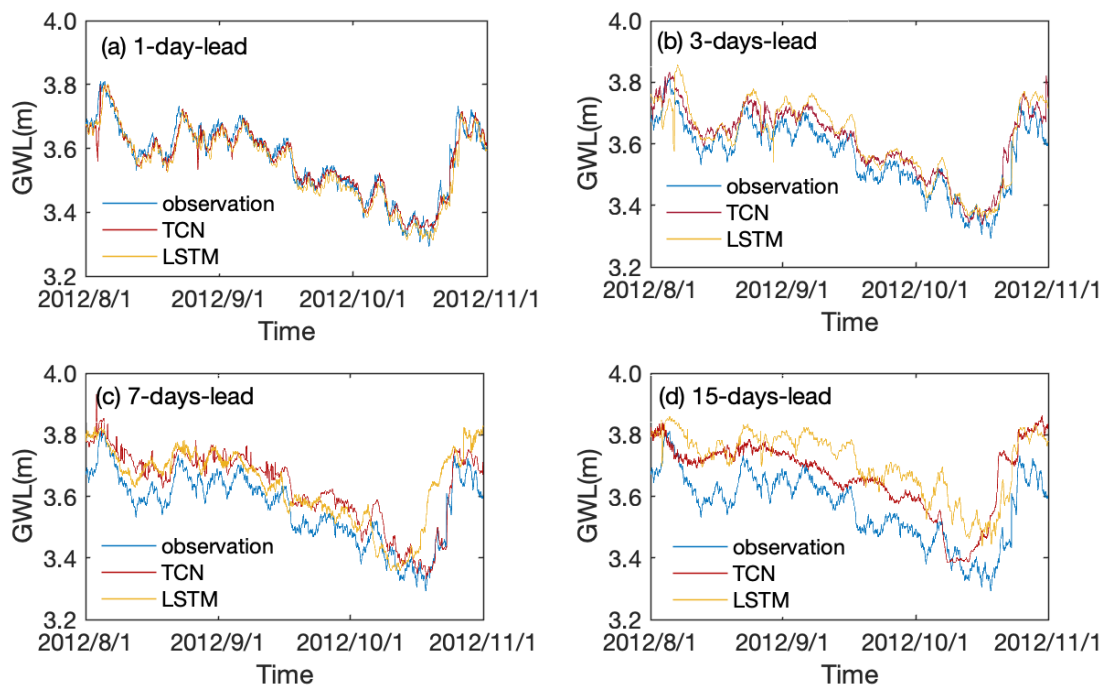
407 Table 3. The model results for groundwater level in the training and testing and  
 408 prediction stage

Well	Model	Training and Testing			Prediction		
		MAE	RMSE	R <sup>2</sup>	MAE	RMSE	R <sup>2</sup>
BH01	TCN	0.0017	0.0068	0.9992	0.0009	0.0019	0.9997
	LSTM	0.0053	0.0077	0.9990	0.0050	0.0074	0.9957
BH05	TCN	0.0070	0.0279	0.9981	0.0061	0.0166	0.9990
	LSTM	0.0082	0.0116	0.9997	0.0168	0.0558	0.9980

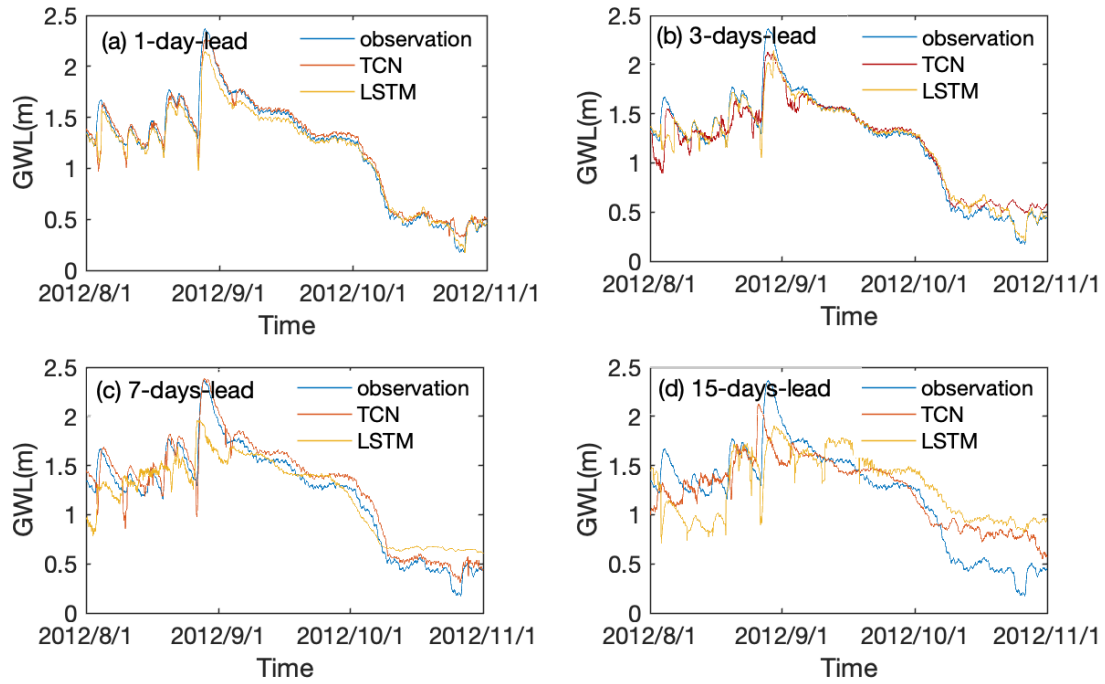
409

410 **4.4 Long term leading time prediction**

411 The TCN- and LSTM-based models were further adjusted to predict the  
412 groundwater levels over three months ahead with different leading period. Prediction  
413 results with 1-day, 3-, 7-, and 15-days leading time with TCN- and LSTM-based models  
414 are illustrated in Fig. 8 and Fig. 9 for wells BH01 and BH05, respectively. The results  
415 show that the predicted groundwater values have the same change trend as the actual  
416 groundwater level in monitoring wells. Both of the models are able to capture the  
417 variation trend of groundwater levels with longer leading period more than one time  
418 step in the two monitoring wells.



419  
420 Figure 8. The observed and predicted values of the groundwater level with TCN- and  
421 LSTM-based models for 1-day, 3-, 7- and 15-days lead period in monitoring well BH01.  
422



423

424 Figure 9. The observed and predicted values of the groundwater level with TCN- and  
 425 LSTM-based models for 1-day, 3-, 7- and 15-days leading period in monitoring well  
 426 BH05.

427 To quantitatively compare the prediction accuracy of the proposed TCN- and  
 428 LSTM-based models, the results of two evaluation metrics with the model running time  
 429 are summarized in Table 4. It can be learned that the  $R^2$  value of TCN-based models  
 430 decreased from 0.9386 to -0.1407 for well BH01 and from 0.9670 to 0.7271 for well  
 431 BH05. Correspondingly, an increase of RMSE values from 0.028 to 0.1209 and 0.0934  
 432 to 0.206 are observed for BH01 and BH05, separately. A similar variation pattern is  
 433 recognized for LSTM-based model with smaller  $R^2$  and higher RMSE than that of the  
 434 TCN-based model. Notably, the running time of advance prediction is much longer than  
 435 that of single step prediction. Meanwhile, with the increasing of leading period, the  
 436 time had been raised nonlinearly. Further, in this process, the TCN-based model cost  
 437 longer time than that of LSTM-based model.



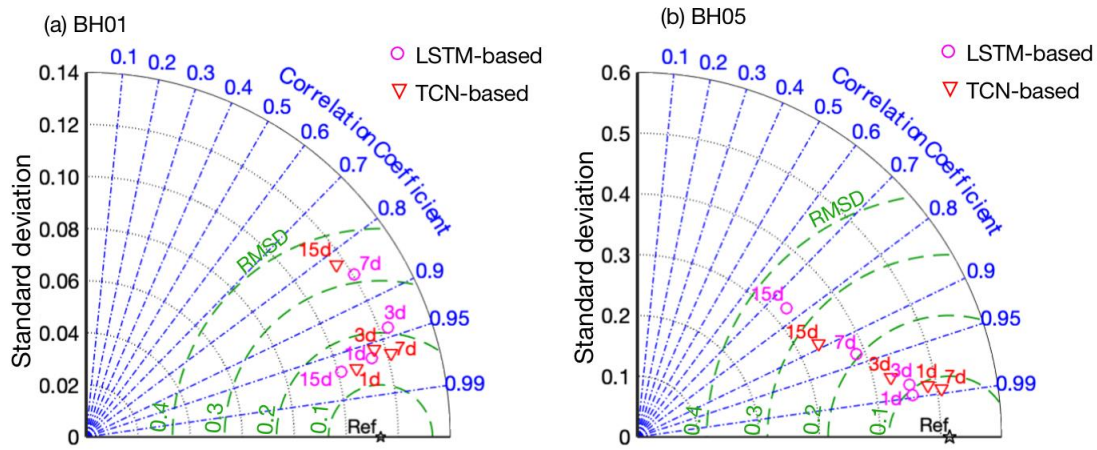
438

Table 4. The model results for groundwater level in the long term prediction

Well	Model	Prediction		Mins	Model	Prediction		Mins
		RMSE	R <sup>2</sup>			RMSE	R <sup>2</sup>	
BH01	TCN-1	0.0280	0.9386	5.38	LSTM-1	0.0349	0.9047	3.76
	TCN-3	0.0550	0.7638	16.1	LSTM-3	0.0640	0.6802	11.01
	TCN-7	0.0741	0.5713	34.3	LSTM-7	0.0956	0.2874	26.27
	TCN-15	0.1209	-0.1407	94.95	LSTM-15	0.1486	-0.7227	85.13
BH05	TCN-1	0.0934	0.9670	5.19	LSTM-1	0.1012	0.9613	3.78
	TCN-3	0.1375	0.9285	16.18	LSTM-3	0.1086	0.9554	11.4
	TCN-7	0.1084	0.9296	35.44	LSTM-7	0.2050	0.8406	26.2
	TCN-15	0.2060	0.7271	80.46	LSTM-15	0.3515	0.5330	73.45

439

440 The performance of the two networks was further evaluated with Taylor diagrams  
441 by taking different criteria aspects which including standard deviation (SD), correlation  
442 coefficient (COR), root mean square deviation (RMSD) into account (Taylor, 2001).  
443 The comparisons of TCN- and LSTM-based model are shown in Fig. 10. As the metrics  
444 distributed away from the reference point (Ref), the deviation of prediction from  
445 observation is generally increased with extending of leading period. Taken well BH05  
446 for example, the prediction with 1-day (24 hours prediction window) in advance are the  
447 highest in agreement with the actual situation in the two models. The 1-day leading  
448 prediction results have the lowest RMSD values and highest R<sup>2</sup> values for both models.  
449 The prediction precision gradually decreases with the extending of leading time to 3-  
450 days, 7-days and 15-days. For well BH01, an out of trending point is observed. The 15-  
451 days prediction results of LSTM-based model is closer to the Ref point compared with  
452 the TCN-based model. The reason is that the simulation data is highly correlated with  
453 observations as shown in Fig.8.



454

455 Figure 10. Taylor diagrams with statistical (SD, COR,RMSD) comparison results of  
 456 the TCN-based and LSTM-based models for well (a) BH01 (b) BH05.

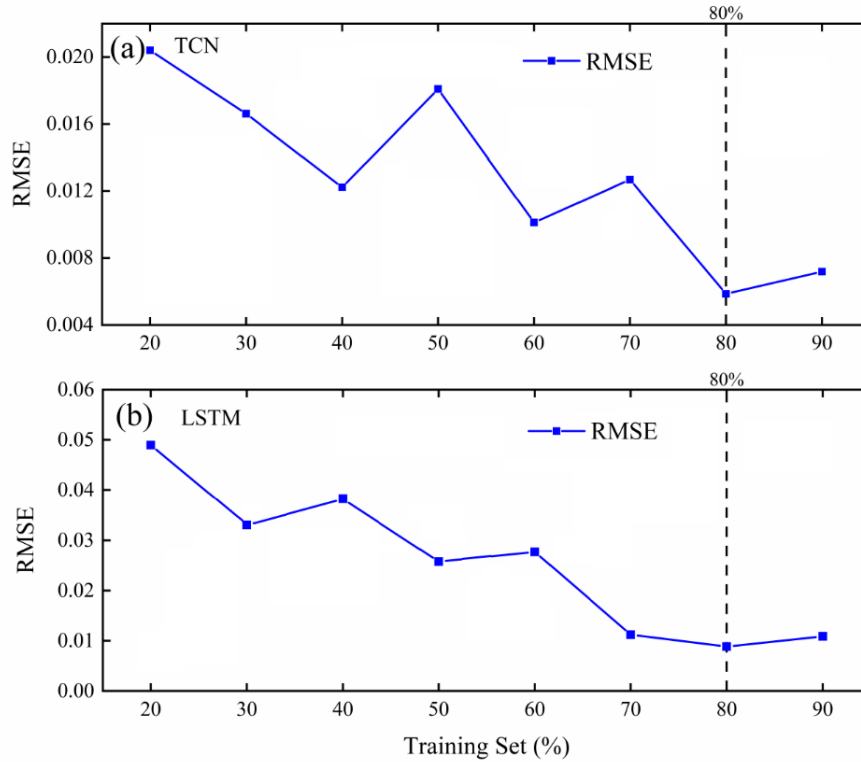
457 Overall, the TCN- and LSTM-based models both have strong prediction ability in  
 458 long term hydrological time series data. Both models are able to provide accurate  
 459 predictions once they are trained. The simulation accuracy of the TCN-based model is  
 460 slightly better than that of the LSTM-based model in the three months prediction but  
 461 the difference is not significant with  $p > 0.05$  in t-test. The causal dilated convolutions  
 462 used by TCNs are proved to be good at capturing long-term dependencies of time series  
 463 data. Meanwhile, the model precision decreases and the running time increases with  
 464 raising leading period. The processing speed of parallel convolution TCN-based models  
 465 for long input sequences is slower than that of recurrent networks. This seems to be a  
 466 shortage in real-time monitoring and early warning. A leading period shorter than 7  
 467 days is recommended to ensure both of the accuracy and efficiency of the models in  
 468 real-time monitoring and early warning.

469 **4.5 Influence of training set percentage**

470 The data-driven methods are supported by data; however, how much data is needed

471 to build an effective model is still a challenging problem (Reichstein et al., 2019). This  
472 is because specific problems depend on application cases, data features, and model  
473 features (Wunsch et al., 2021). Here we discuss the effect of training set percentage on  
474 the TCN- and LSTM-based models. In our study, the data is the hourly-monitored data  
475 from 2011 to 2012. From 2011, we set 20%, 30% to 90% training sets in turn, so as to  
476 gradually expand the length of training set.

477 Fig. 11 shows the effect of increased percentage of training set on the performance  
478 of the model. All experiments were repeated five times, and the average values of each  
479 index were compared. It can be seen that the performance of the TCN-based model  
480 improved with the increase of the percentage of training set. When the training set  
481 reached 80%, the performance was relatively optimal, and then the performance began  
482 to deteriorate with the increase of the percentage of training set. At the same time, it  
483 can be seen that the performance of the LSTM-based model tends to be stable when the  
484 training set reaches 70%, and then decreases slightly with the increase of training set.  
485 Therefore, a training set evaluation is recommended before the training and testing. We  
486 should carefully evaluate and shorten the training data set as much as possible when  
487 necessary. Finally, we set 80% of the training set length to simulate the coastal aquifer  
488 time-series data.



489

490 Figure 11. Influence of training set percentage on the performance of the model for (a)  
 491 BH01 and (b) BH05.

## 492 5 Conclusions

493 The TCN- and LSTM-based deep learning models were proposed in this paper to  
 494 predict groundwater levels in a coastal aquifer. Hyper-parameter searches was first  
 495 conducted to obtain good architecture configurations. The results indicated that a deeper,  
 496 broader model does not necessarily guarantee better predictions. The optimal  
 497 configurations then were adopted for the networks of all monitoring data. Both of the  
 498 TCN- and LSTM- based model well captured the fluctuation of groundwater levels and  
 499 achieved satisfactory performance on the prediction. Meanwhile, a decreasing precision  
 500 is revealed when the leading time increases in advance prediction. In view of accuracy,  
 501 the TCN-based model outperforms the LSTM-based model but less efficiency in long-

502 term simulation. Thus, both models can be used as promising method for time-series  
503 prediction of hydrogeological data especially when the regional data is difficult to  
504 collect in a complex system.

#### 505 **Acknowledgements**

506 This work was jointly supported by National Natural Science Foundation of  
507 China (No: 41702244), the Program for Jilin University (JLU) Science and Technology  
508 Innovative Research Team (No. 2019TD-35).

#### 509 **Code availability**

510 The pieces of code that were used for all analyses are available from the authors  
511 upon request.

#### 512 **Data availability**

513 The data sets that have been analyzed in this paper are available from the  
514 authors upon request.

#### 515 **Author contribution**

516 XZ drafted the manuscript and revised the manuscript. GC designed the  
517 experiments and collected all the data. DF developed the model code and performed  
518 the simulations. ZD was responsible for the project design, oversaw the analysis, and  
519 conducted manuscript revision as the project leader and the senior scientist.

#### 520 **Competing interests**

521 The authors declare that they have no conflict of interest.

#### 522 **Reference**

523 Abdalla, O. A. and Al-Rawahi, A. S.: Groundwater recharge dams in arid areas as tools  
524 for aquifer replenishment and mitigating seawater intrusion: example of AlKhod,

525 Oman, *Environ. Earth Sci.*, 69, 1951-1962, 2013.

526 Adam, D. K. J. B.: A method for stochastic optimization in: 3rd International  
527 Conference on Learning Representations, 2015.

528 Afaq, S. and Rao, S.: Significance of epochs on training a neural network, *International*  
529 *Journal of Scientific & Technology Research*, 9, 485-488, 2020.

530 Baena-Ruiz, L., Pulido-Velazquez, D., Collados-Lara, A.-J., Renau-Pruñonosa, A., and  
531 Morell, I.: Global assessment of seawater intrusion problems (status and  
532 vulnerability), *Water Resour. Manag.*, 32, 2681-2700, 2018.

533 Bai, S., Kolter, J. Z., and Koltun, V.: An empirical evaluation of generic convolutional  
534 and recurrent networks for sequence modeling, arXiv preprint arXiv:1803.01271,  
535 2018.

536 Barlow, P. M. and Reichard, E. G.: Saltwater intrusion in coastal regions of North  
537 America, *Hydrogeol. J.*, 18, 247-260, 2010.

538 Batelaan, O., De Smedt, F., and Triest, L.: Regional groundwater discharge:  
539 phreatophyte mapping, groundwater modelling and impact analysis of land-use  
540 change, *J. Hydrol.*, 275, 86-108, 2003.

541 Bengio, Y., Simard, P., and Frasconi, P.: Learning long-term dependencies with gradient  
542 descent is difficult, *IEEE Trans. Neural Netw.*, 5, 157-166, 1994.

543 Borovykh, A., Bohte, S., and Oosterlee, C. W.: Dilated convolutional neural networks  
544 for time series forecasting, *J. Comput. Financ.*, 2018.

545 Cannas, B., Fanni, A., See, L., and Sias, G.: Data preprocessing for river flow  
546 forecasting using neural networks: wavelet transforms and data partitioning, *Phys.*  
547 *Chem. Earth*, 31, 1164-1171, 2006.

548 Cao, Y., Ding, Y., Jia, M., and Tian, R.: A novel temporal convolutional network with  
549 residual self-attention mechanism for remaining useful life prediction of rolling  
550 bearings, *Reliab. Eng. Syst. Saf.*, 215, 107813, 2021.

551 Chen, Y., Kang, Y., Chen, Y., and Wang, Z.: Probabilistic forecasting with temporal  
552 convolutional neural network, *Neurocomputing*, 399, 491-501, 2020.

553 Coulibaly, P., Anctil, F., Aravena, R., and Bobée, B.: Artificial neural network modeling  
554 of water table depth fluctuations, *Water Resour. Res.*, 37, 885-896, 2001.

555 Dai, Z. and Samper, J.: Inverse modeling of water flow and multicomponent reactive  
556 transport in coastal aquifer systems, *J. Hydrol.*, 327, 447-461, 2006.

557 Dai, Z., Xu, L., Xiao, T., McPherson, B., Zhang, X., Zheng, L., Dong, S., Yang, Z.,  
558 Soltanian, M. R., and Yang, C.: Reactive chemical transport simulations of geologic  
559 carbon sequestration: Methods and applications, *Earth-Sci. Rev.*, 208, 103265, 2020.

560 Dubey, A. K., Kumar, A., García-Díaz, V., Sharma, A. K., and Kanhaiya, K.: Study and  
561 analysis of SARIMA and LSTM in forecasting time series data, *Sustain. Energy*  
562 *Technol. Assess.*, 47, 101474, 2021.

563 Ergen, T. and Kozat, S. S.: Efficient online learning algorithms based on LSTM neural  
564 networks, *IEEE Trans. Neural Netw. Learn. Syst.*, 29, 3772-3783, 2017.

565 Feng, N., Geng, X., and Qin, L.: Study on MRI medical image segmentation technology  
566 based on CNN-CRF model, *IEEE Access*, 8, 60505-60514, 2020.

567 Fischer, T. and Krauss, C.: Deep learning with long short-term memory networks for  
568 financial market predictions, *Eur. J. Oper. Res.*, 270, 654-669, 2018.

569 Gan, Z., Li, C., Zhou, J., and Tang, G.: Temporal convolutional networks interval  
570 prediction model for wind speed forecasting, *Electr. Power Syst. Res.*, 191, 106865,  
571 2021.

572 Garza-Díaz, L. E., DeVincentis, A. J., Sandoval-Solis, S., Azizipour, M., Ortiz-Partida,  
573 J. P., Mahlknecht, J., Cahn, M., Medellín-Azuara, J., Zaccaria, D., and Kisekka, I.:  
574 Land-use optimization for sustainable agricultural water management in Pajaro  
575 Valley, California, *J. Water Resour. Plan. Manage.-ASCE*, 145, 05019018-  
576 05019018, 2019.

577 Gorgij, A. D., Kisi, O., and Moghaddam, A. A.: Groundwater budget forecasting, using  
578 hybrid wavelet-ANN-GP modelling: a case study of Azarshahr Plain, East  
579 Azerbaijan, Iran, *Hydrol. Res.*, 48, 455-467, 2017.

580 Han, D., Kohfahl, C., Song, X., Xiao, G., and Yang, J.: Geochemical and isotopic  
581 evidence for palaeo-seawater intrusion into the south coast aquifer of Laizhou Bay,  
582 China, *Appl. Geochem.*, 26, 863-883, 2011.

583 Han, D., Song, X., Currell, M. J., Yang, J., and Xiao, G.: Chemical and isotopic  
584 constraints on evolution of groundwater salinization in the coastal plain aquifer of  
585 Laizhou Bay, China, *J. Hydrol.*, 508, 12-27, 2014.

586 He, K., Zhang, X., Ren, S., and Sun, J.: Deep residual learning for image recognition,  
587 *Proc. IEEE*, 770-778,

588 Huang, F.-K., Chuang, M.-H., Wang, G. S., and Yeh, H.-D.: Tide-induced groundwater  
589 level fluctuation in a U-shaped coastal aquifer, *J. Hydrol.*, 530, 291-305, 2015.

590 Jiang, Y., Zhao, M., Zhao, W., Qin, H., Qi, H., Wang, K., and Wang, C.: Prediction of  
591 sea temperature using temporal convolutional network and LSTM-GRU network,  
592 *Complex Engineering Systems*, 1, -, 2021.

593 Ketabchi, H. and Ataie-Ashtiani, B.: Evolutionary algorithms for the optimal  
594 management of coastal groundwater: A comparative study toward future challenges,  
595 *J. Hydrol.*, 520, 193-213, 2015.

596 Kratzert, F., Herrnegger, M., Klotz, D., Hochreiter, S., and Klambauer, G.:  
597 NeuralHydrology—interpreting LSTMs in hydrology, in: *Explainable AI:  
598 Interpreting, explaining and visualizing deep learning*, Springer, 347-362, 2019.

599 Kreyenberg, P. J., Bauser, H. H., and Roth, K.: Velocity field estimation on density-  
600 driven solute transport with a convolutional neural network, *Water Resour. Res.*, 55,  
601 7275-7293, 2019.

602 Lara-Benítez, P., Carranza-García, M., Luna-Romera, J. M., and Riquelme, J. C.:  
603 Temporal convolutional networks applied to energy-related time series forecasting,  
604 *applied sciences*, 10, 2322, 2020.

605 Lea, C., Vidal, R., Reiter, A., and Hager, G. D.: Temporal convolutional networks: A  
606 unified approach to action segmentation, *European conference on computer vision*,  
607 47-54,

608 Lea, C., Flynn, M. D., Vidal, R., Reiter, A., and Hager, G. D.: Temporal convolutional  
609 networks for action segmentation and detection, *Proc. IEEE*, 156-165,

610 LeCun, Y., Bottou, L., Bengio, Y., and Haffner, P.: Gradient-based learning applied to  
611 document recognition, *Proc. IEEE*, 86, 2278-2324, 1998.

612 Li, H., Jiao, J. J., Luk, M., and Cheung, K.: Tide-induced groundwater level fluctuation

613 in coastal aquifers bounded by L-shaped coastlines, *Water Resour. Res.*, 38, 6-1-6-  
614 8, 2002.

615 Long, J., Shelhamer, E., and Darrell, T.: Fully convolutional networks for semantic  
616 segmentation, *Proc. IEEE*, 3431-3440,

617 Lu, C., Werner, A. D., and Simmons, C. T.: Threats to coastal aquifers, *Nature Climate*  
618 *Change*, 3, 605-605, 2013.

619 Lu, C., Cao, H., Ma, J., Shi, W., Rathore, S. S., Wu, J., and Luo, J.: A proof-of-concept  
620 study of using a less permeable slice along the shoreline to increase fresh  
621 groundwater storage of oceanic islands: Analytical and experimental validation,  
622 *Water Resour. Res.*, 55, 6450-6463, 2019.

623 Maier, H. R. and Dandy, G. C.: Neural networks for the prediction and forecasting of  
624 water resources variables: a review of modelling issues and applications, *Environ.*  
625 *Modell. Softw.*, 15, 101-124, 2000.

626 Mehr, A. D. and Nourani, V.: A Pareto-optimal moving average-multigene genetic  
627 programming model for rainfall-runoff modelling, *Environ. Modell. Softw.*, 92,  
628 239-251, 2017.

629 Mei, Y., Tan, G., and Liu, Z.: An improved brain-inspired emotional learning algorithm  
630 for fast classification, *Algorithms*, 10, 70, 2017.

631 Nair, V. and Hinton, G. E.: Rectified linear units improve restricted boltzmann machines,  
632 *Icml*,

633 Park, Y., Lee, J.-Y., Kim, J.-H., and Song, S.-H.: National scale evaluation of  
634 groundwater chemistry in Korea coastal aquifers: evidences of seawater intrusion,  
635 *Environ. Earth Sci.*, 66, 707-718, 2012.

636 Pascanu, R., Mikolov, T., and Bengio, Y.: On the difficulty of training recurrent neural  
637 networks, *International conference on machine learning*, 1310-1318, 2013.

638 Pratheepa, V., Ramesh, S., Sukumaran, N., and Murugesan, A.: Identification of the  
639 sources for groundwater salinization in the coastal aquifers of Southern Tamil Nadu,  
640 India, *Environ. Earth Sci.*, 74, 2819-2829, 2015.

641 Reichstein, M., Camps-Valls, G., Stevens, B., Jung, M., Denzler, J., and Carvalhais, N.:  
642 Deep learning and process understanding for data-driven Earth system science,  
643 *Nature*, 566, 195-204, 2019.

644 Rumelhart, D. E., Hinton, G. E., and Williams, R. J.: Learning representations by back-  
645 propagating errors, *Nature*, 323, 533-536, 1986.

646 Sahoo, S., Russo, T., Elliott, J., and Foster, I.: Machine learning algorithms for  
647 modeling groundwater level changes in agricultural regions of the US, *Water Resour.*  
648 *Res.*, 53, 3878-3895, 2017.

649 Salimans, T. and Kingma, D. P.: Weight normalization: A simple reparameterization to  
650 accelerate training of deep neural networks, *Advances in neural information*  
651 *processing systems*, 29, 2016.

652 Senthil Kumar, A., Sudheer, K., Jain, S., and Agarwal, P.: Rainfall-runoff modelling  
653 using artificial neural networks: comparison of network types, *Hydrological*  
654 *Processes: An International Journal*, 19, 1277-1291, 2005.

655 Seo, Y., Kim, S., Kisi, O., and Singh, V. P.: Daily water level forecasting using wavelet  
656 decomposition and artificial intelligence techniques, *J. Hydrol.*, 520, 224-243, 2015.



657 Solgi, R., Loáiciga, H. A., and Kram, M.: Long short-term memory neural network  
658 (LSTM-NN) for aquifer level time series forecasting using in-situ piezometric  
659 observations, *J. Hydrol.*, 601, 126800, 2021.

660 Srivastava, N., Hinton, G., Krizhevsky, A., Sutskever, I., and Salakhutdinov, R.:  
661 Dropout: a simple way to prevent neural networks from overfitting, *J. Mach. Learn.*  
662 *Res.*, 15, 1929-1958, 2014.

663 Taylor, K. E.: Summarizing multiple aspects of model performance in a single diagram,  
664 *J. Geophys. Res.-Atmos.*, 106, 7183-7192, 2001.

665 Torres, J. F., Troncoso, A., Koprinska, I., Wang, Z., and Martínez-Álvarez, F.: Deep  
666 learning for big data time series forecasting applied to solar power, *The 13th*  
667 *International Conference on Soft Computing Models in Industrial and*  
668 *Environmental Applications*, 123-133, 2018.

669 Wan, R., Mei, S., Wang, J., Liu, M., and Yang, F.: Multivariate temporal convolutional  
670 network: A deep neural networks approach for multivariate time series forecasting,  
671 *Electronics*, 8, 876, 2019.

672 Wunsch, A., Liesch, T., and Broda, S.: Groundwater level forecasting with artificial  
673 neural networks: a comparison of long short-term memory (LSTM), convolutional  
674 neural networks (CNNs), and non-linear autoregressive networks with exogenous  
675 input (NARX), *Hydrol. Earth Syst. Sci.*, 25, 1671-1687, 2021.

676 Xu, Z. and Hu, B. X.: Development of a discrete-continuum VDFST-CFP numerical  
677 model for simulating seawater intrusion to a coastal karst aquifer with a conduit  
678 system, *Water Resour. Res.*, 53, 688-711, 2017.

679 Xue, Y., Wu, J., Ye, S., and Zhang, Y.: Hydrogeological and hydrogeochemical studies  
680 for salt water intrusion on the south coast of Laizhou Bay, China, *Groundwater*, 38,  
681 38-45, 2000.

682 Yan, J., Mu, L., Wang, L., Ranjan, R., and Zomaya, A. Y.: Temporal convolutional  
683 networks for the advance prediction of ENSO, *Sci Rep*, 10, 1-15, 2020.

684 Zeng, X., Wu, J., Wang, D., and Zhu, X.: Assessing the pollution risk of a groundwater  
685 source field at western Laizhou Bay under seawater intrusion, *Environ. Res.*, 148,  
686 586-594, 2016.

687 Zhan, C., Dai, Z., Soltanian, M. R., and Zhang, X.: Stage-wise stochastic deep learning  
688 inversion framework for subsurface sedimentary structure identification, *Geophys.*  
689 *Res. Lett.*, 49, e2021GL095823, 2022.

690 Zhang, D., Lin, J., Peng, Q., Wang, D., Yang, T., Sorooshian, S., Liu, X., and Zhuang,  
691 J.: Modeling and simulating of reservoir operation using the artificial neural  
692 network, support vector regression, deep learning algorithm, *J. Hydrol.*, 565, 720-  
693 736, 2018a.

694 Zhang, J., Zhu, Y., Zhang, X., Ye, M., and Yang, J.: Developing a Long Short-Term  
695 Memory (LSTM) based model for predicting water table depth in agricultural areas,  
696 *J. Hydrol.*, 561, 918-929, 2018b.

697 Zhang, J., Zhang, X., Niu, J., Hu, B. X., Soltanian, M. R., Qiu, H., and Yang, L.:  
698 Prediction of groundwater level in seashore reclaimed land using wavelet and  
699 artificial neural network-based hybrid model, *J. Hydrol.*, 577, 123948, 2019.

700 Zhang, X., Miao, J., Hu, B. X., Liu, H., Zhang, H., and Ma, Z.: Hydrogeochemical

701 characterization and groundwater quality assessment in intruded coastal brine  
702 aquifers (Laizhou Bay, China), *Environ. Sci. Pollut. Res.*, 24, 21073-21090, 2017.  
703 Zhang, X., Dong, F., Dai, H., Hu, B. X., Qin, G., Li, D., Lv, X., Dai, Z., and Soltanian,  
704 M. R.: Influence of lunar semidiurnal tides on groundwater dynamics in estuarine  
705 aquifers, *Hydrogeol. J.*, 28, 1419-1429, 2020.  
706